University of Sistan and Baluchestan

Chemical Process Design

Available online at http://cpd.usb.ac.ir/

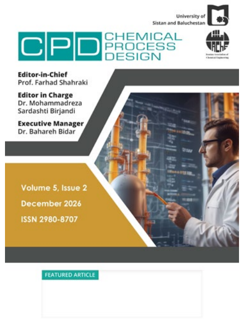

Modeling and statistical analysis on the viscosity of aqueous solution of xanthan gum as drag reducing agent using RSM

Behrouz Raei[1]✉

[1] Department of Chemical Engineering, Mahs. C., Islamic Azad University, Mahshahr, Iran. Email: behrouz.raei@iau.ac.ir

ARTICLE INFO

Article type:
Research Article

Article history:
Received: 2026-01-31
Received in revised form: 2026-07-16
Accepted: 2026-07-28
Available online: 2026-07-28

Keywords: *Viscosity; Xanthan gum; Response surface methodology; Drag reduction*

ABSTRACT

Polymeric drag-reducing agents (DRAs) have shown significant advantages for industrial applications following over seven decades of study. An experiment and statistical study were carried out to develop an equation for the viscosity of XG solution in water as a DRA using response surface methodology (RSM). The research was conducted under experimental settings with a concentration range of C=50-1000 ppm and temperature between T=30-50°C. Different models were evaluated based on a series of quality metrics and plots. After examining the quality metrics and plots of different models, it was concluded that the quadratic model was the most appropriate choice. The values of standard deviation (Std.Dev), coefficient of determination (R^2) and coefficient of variation (C.V) for the quadratic model were 0.0001, 0.9959, and 4.37, respectively. The outcomes of the RSM model were compared with 6 equations found in the literature. The results indicated that the RSM model had the smallest average absolute relative deviation (AARD=5.39%) when estimating the dynamic viscosity of aqueous XG solution. Finally, the prediction quality of the RSM model was examined with experimental data from literature. The results showed that the proposed equation can predict the viscosity of water-soluble DRAs with acceptable accuracy with a relative deviation of less than 19%. The application of RSM cuts down on experimental costs and time, in addition to helping identify the most suitable model.

Cite this article: Raei, B., (2026), Modeling and statistical analysis on the viscosity of aqueous solution of xanthan gum as drag reducing agent using RSM, *Chemical Process Design*, 5(2), 00-00. http//doi.org/10.22111/cpd.2026.54615.1084

DOI: http//doi.org/10.22111/cpd.2026.54615.1084

Publisher: University of Sistan and Baluchestan.

1. Introduction

Adding a small amount of high molecular weight polymer (also known as a drag-reducing agent, or DRA) to turbulent water flow can significantly lower skin frictional drag. This was first noted by Toms in 1948 [1]. In the last seventy years, thorough investigations have resulted in the common use of polymer additives across various sectors, including pipeline transportation, fire control, biomedical uses, and irrigation [2]. The additive drag reduction method may reduce safety risks, lower construction costs for pipelines and pump stations, reduce operating and maintenance costs, and transform inflexible pipeline capacity into flexible pipeline capacity. Consequently, it can be determined that wisely using a drag reducer is more economical. The primary mechanisms underlying DRA are altering the mean velocity profile, altering the turbulent vorticity, and redistributing the stresses through the extension and relaxation of long-chain molecules in the near-wall region. As a result, this change lessens momentum transfer from the free-stream to the wall, which eventually lowers skin friction [3, 4].

Flexible polymers, typically synthetic like polyethylene oxide (PEO) and polyacrylamide (PAM) [5, 6], or rigid molecules, like the biopolymers xanthan gum (XG) and diutan gum (DG), can be used to formulate polymer solutions for drag reduction [7]. Although turbulent drag can be significantly lowered by both of these additives, the suggested mechanisms for drag reduction seem to be different.

Flexible polymers are generally preferred for DR usages because they significantly reduce drag at a low concentration without significantly raising the fluid's viscosity. Conversely, there has been less focus on rigid polymer solutions. Rigid polymer solutions need significantly higher concentrations than flexible polymers to achieve high ranks of DR, which is one of the main distinctions seen in experiments [8, 9]. Furthermore, the resistance of rigid polymeric fluids to mechanical scission (or degradation) in turbulent flow is different from that of flexible ones [2, 10, 11]. Actually, rather than molecular scission, degradation in rigid polymers seems to be caused by aggregate destruction [11].

Numerous studies show that various factors, such as the molecular weight (Mw), the type and concentration of the polymer, the polymer degradation, the type of solution preparation, the solvent properties, the temperature of the solution, and more, have a significant impact on the ability of polymers to reduce friction in turbulent flow. [12]. Since the first findings about friction reducing polymers, many investigations have been carried out in this area. Mohammadtabar et al. [6] accomplished 40%–50% drag reduction in pipeline devices by effectively employing various water-soluble polymers, including PAM, PEO, XG, and carboxymethyl cellulose (CMC). The results of the research demonstrated that rigid polymers have better shear resistance than flexible polymers but a lower rate of drag reduction. Lim [13] examined the decrease in turbulence drag by using XG, a polymer that possesses diverse structures, in a water-based solution. The results of the experiment showed that the DR% for XG rose with higher polymer concentrations but decreased in high shear conditions. Sandoval et al. [14] used a pipeline apparatus to examine the DR efficiency of PEO, PAM, and XG. They discovered considerable synergistic interactions among the polymers. In order to study DR and degradation, Rajappan & McKinley [15] examined the polysaccharide that was extracted from the mucilage. This polysaccharide was found to decrease friction in turbulent flow by as much as 15%. According to the latest research, references [16-27] can be cited.

Xanthan gum (XG) is a biopolymer generated by the aerobic fermentation of glucose or sucrose utilizing the bacterium *Xanthomonas campestris* [28]. Because of its viscosifying characteristics, this biopolymer is highly adaptable and utilized in numerous industrial applications [29]. Additionally, it serves as a thickening agent, emulsion stabilizer, or suspending agent across various sections including food, pharmaceuticals, cosmetics, textiles, agriculture, and petroleum, especially in the formulation of drilling fluids and as a DRA [30, 31]. An overview of earlier research on the application of XG as a DRA in aqueous solution is provided in Table 1.

Table 1. Review of using XG as a DRA in previous studies

Investigator	Year	Base fluid	Operating conditions	Experimental system	Mw (g/mol)
Raei & Peyghambarzadeh [32]	2021	Deionized water	C :100-1000 ppm T :30-50 °C	Pipelines	4.5×10^6
Li et al. [33]	2024	Water	C:500-5000 ppm T :10-60 °C	Ring vacuum pump	10^6
Abdulbari et al. [34]	2018	Deionized water	C :20-500 ppm	Microchannel	4.5×10^6
Abdulbari & Amir [35]	2021	Distilled water	C :50-250 ppm	Rotating disk apparatus	NA
Li et al. [36]	2022	Water	C :100-500 ppm T :25 °C	Pipe flow	2×10^6-7×10^6
Karami et al. [37]	2018	Deionized water, Tab water	C :50-300 ppm	Pipe flow	2×10^6
Choi et al. [38]	2000	Deionized water	C :10-200 ppm T :25 °C	Rotating disk apparatus	NA
Habibpour & Clark [39]	2017	Deionized water	C :600 ppm T :25 C	Pipe flow	4-5×10^6
Mohammadtabar et al. [6]	2020	Distilled water	C :50 ppm T :25 °C	Pipe flow	2-5×10^6
Gustavo et al. [14]	2016	Filtered water	C :50-200 ppm T :25 °C	Pipe flow	2×10^6
Mitishita et al. [40]	2023	Tap water	C :150-1500 ppm T :23 C	Rectangular duct	NA
Novelli et al. [41]	2019	Water	C :100 ppm T :20 °C	Rotational rheometer	1.96×10^6
Habibpour et al. [42]	2017	Deionized water	C :300-1000 ppm T :25 C	Pipe flow	4-5×10^6
Akindoyo & Abdulbari [43]	2016	Deionized water	C :65-105 ppm T :25-40 °C	Rotating disk apparatus	2×10^6
Pereira et al. [11]	2013	Deionized water	C :100-1000 ppm T :20-50 °C	Rotating cylindrical double gap device	2×10^6

It has been determined that viscosity is the most critical characteristics property of working fluids with DRA, as its variation is not negligible [44, 45]. As far as was investigated, no independent and comprehensive study has been conducted on the viscosity of DRA. Also, there is no specific equation available to calculate the viscosity of DRA. On the other hand, although many experimental, theoretical, and numerical studies have been conducted on DRA, very limited studies have been conducted on the statistical analysis of DR, including the following references [46-48]. The innovation of the present research is the empirical investigation and statistical analysis of the viscosity of the aqueous XG solution as DRA using RSM and the presentation of an equation for predicting the viscosity of DRA. Another objective of this study is to compare the proposed equation with other equations in the literature.

2. Materials and Methods

2.1. Materials

Without undergoing further purification, XG powder from Sigma-Aldrich was used. Because of its good shear ability, it is widely used in the petroleum industry for enhanced oil recovery and as a DRA. The biopolymer's specifications are displayed in Table 2.

2.2. Preparation of XG solution

The preparation steps are as follows: First, gradually add the measured XG powder into a container with water while stirring rapidly and consistently. After that, it stood for 36h until it was entirely dissolved. Next, the mother liquid should be transferred into the liquid reservoir, and the solution must be agitated rapidly and uniformly. It should be permitted to remain undisturbed for a period of 24h before its utilization in the experimental procedure.

Table 2. Specifications of XG used in this study

Name (Formula)	Chemical Structure	Mw (g/mol)	Appearance (Color)	Form	Brookfield Viscosity (1% Solution) cps
Xanthan Gum, $C_{35}H_{49}O_{29}$ (monomer)	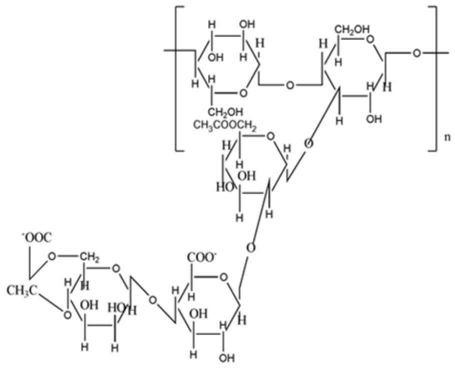	4.5×10^{6}	Faint Yellow to Yellow to Beige	Powder	800-1200

2.3. Measurement of viscosity

The apparatus shown in Fig. 1 has been set up for the purpose of measuring the viscosity of XG solution. In this kind of viscometer, the viscosity is assessed by timing how long it takes for a specific volume of the tested liquid to pass through a capillary tube, driven by gravitational force, while maintaining a constant temperature. The device incorporates an Ostwald viscometer placed within a temperature-regulated water bath (MATEST model B052-01, Italy), which maintains a temperature fluctuation of ±0.5°C. After filling the viscometer with the required amount of test fluid (XG solution), it is allowed to flow between two designated marks, A and B (shown in Fig. 1) through the capillary tube. To ensure accuracy in quantifying time, a stopwatch with an accuracy of 0.01s was employed to meticulously record the elapsed time required to reach each of the markers on the viscometer. After determining the viscosity of the base fluid (*bf*), the viscosity of the XG solution (*p*) was computed using Eq. (1):

$$\frac{\mu_p}{\mu_{bf}}=\frac{\rho_p}{\rho_{bf}}\frac{t_p}{t_{bf}} \tag{1}$$

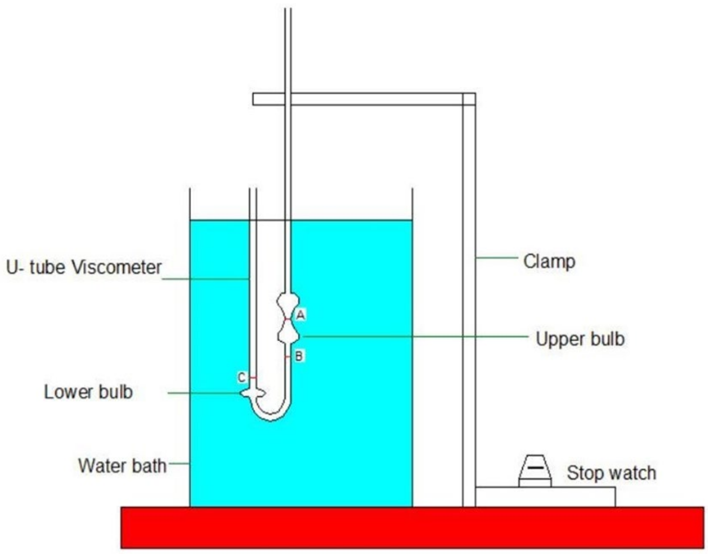

Fig 1. Schematic of the apparatus for viscosity measurement

By measuring the viscosity of distilled water (DW) at the specified test temperatures of 30, 40, and 50°C, the viscometer's calibration was confirmed. The reference data from IAPWS[1] 2008 was compared with the measured viscosity values for DW. The calculated maximum percentage error was determined to be 4.1%. To reduce experimental error and ensure repeatability, every measurement was conducted three times under the identical conditions. The uncertainty associated with measuring the viscosity of the XG solution was determined using the mathematical expressions outlined in Eq. (2) [49]:

$$U_{\mu p} = \pm\sqrt{\left(\frac{\Delta\mu_p}{\mu_p}\right)^2 + \left(\frac{\Delta w}{w}\right)^2 + \left(\frac{\Delta T}{T}\right)^2 + \left(\frac{\Delta t}{t}\right)^2} \tag{2}$$

In this context, U represents the uncertainty associated with the measurements; w indicates the weight of the polymer, and T signifies the temperature. Δ represents the variation in the measurements. The maximum uncertainty calculated was 2.9%. Research assumptions include the following: XG solution homogeneously distributed in the test section and XG concentration is assumed to be uniform and constant.

3. Response Surface Methodology (RSM) modelling

To determine the model's sensitivity, Box and Wilson [50] developed a statistical and mathematical technique called Response Surface Methodology (RSM). It is beneficial for examining issues and fitting models when the dependent variable is influenced by a significantly larger number of independent variables [51]. RSM allows researchers to improve processes while minimizing the number of empirical tests. The RSM-ANOVA technique is an effective means of clarifying the relation between input factors and the output factor. The ability of the RSM-ANOVA technique to handle multiple variables makes it applicable in a variety of ideal situations, and its provision of statistical validation makes it an essential tool in numerous fields. The linear, squared, and two-factor interaction terms of independent parameters (X_i) constitute the response for the second-order mathematical model (Eq. (3)), which is indicated by Gaitonde et al. [52]:

$$Response = d_0 + \sum_{i=1}^{k} d_i X_i + \sum_{i=1}^{k} d_{ii} X_1^2 + \sum_{i=1}^{k-1} \sum_{j=i+1}^{k} d_{ij} X_i X_j \tag{3}$$

where d is the regression coefficient.

4. Results and discussion

4.1. Statistical analysis

Viscosity is a crucial factor in determining how DRA affects flow characteristics. In this research, the viscosity of solutions with XG polymer was measured experimentally at varying concentrations and at three distinct temperatures: 30°C, 40°C, and 50°C, with the outcomes illustrated in Fig. 2. As illustrated in Fig. 2, a rise in the concentration of XG results in a rise in the viscosity of the polymer solution. This phenomenon is particularly noticeable at lower temperatures. It is clear that the viscosity of the XG solution demonstrated a nearly exponential rise as the concentration increased. The findings of the viscosity tests conducted in this research align well with the outcomes reported by Varnaseri and Peyghambarzadeh [53].

[1] International Association for the Properties of Water and Steam (IAPWS)

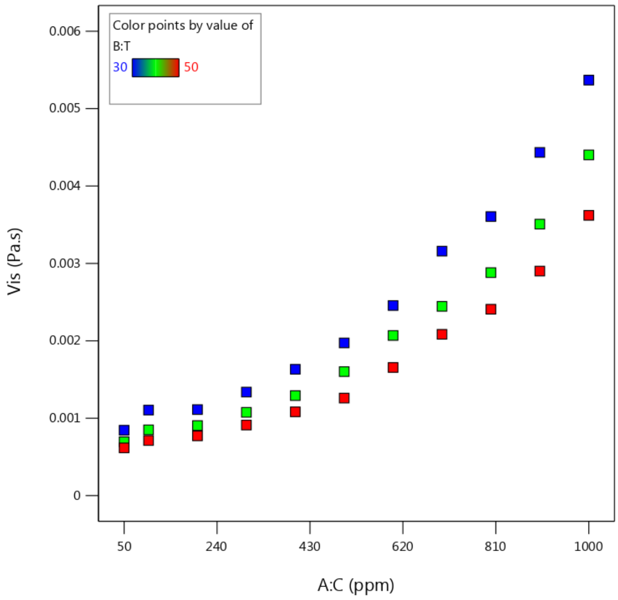

Fig. 2. Viscosity of the aqueous XG solution as a function of concentration and temperature

33 sets of laboratory data were used as historical data to model the viscosity of the aqueous XG solution through the RSM in Design Expert software version 13.0.0. In this context, the concentration and temperature of the polymer solution are treated as independent variables, while the dynamic viscosity is regarded as the dependent variable. Table 3 presents the features of the input variables. The goal of the research is to determine a correlation that can forecast the viscosity of the aqueous XG solution.

Table 3. Specifications of used factors in modeling

Factor	Name	Units	Type	Minimum	Maximum	Coded Low	Coded High	Mean	Std. Dev.
A	C	ppm	Numeric	50.00	1000.00	-1 ↔ 50.00	+1 ↔ 1000.00	504.55	314.09
B	T	C	Numeric	30.00	50.00	-1 ↔ 30.00	+1 ↔ 50.00	40.00	8.29

Based on Table 4, the RSM has created four different models: the linear model, the 2FI model, the quadratic model, and the cubic model. The cubic model is aliased, while the quadratic model is suggested. This indicates that RSM is applicable solely to variables that can be represented by a quadratic equation. The statistical measure known as the *p-value* indicates the likelihood of validating a hypothesis based on the existing data, while also determining the probability of observing the outcomes if the null hypothesis holds true. The *p-value* approaching zero denotes that the model is statistically significant. Moreover, the coefficient of determination (R^2) indicates how well the actual data align with the predicted values. R^2 ranges from 0 to 1, and a value approaching 1 indicates that the model has high precision. The predicted R^2 evaluated the model using values beyond the available observed data range, while the adjusted R^2 took into account the effects of the model's coefficients. The information shown in this table reveals that the quadratic model has the greatest adjusted R^2 value of 0.9951 and a predicted R^2 of 0.9929, indicating that it is the most accurate model.

Table 4. Summary of statistics for the various models.

Source	Sequential p-value	Adjusted R^2	Predicted R^2	
Linear	< 0.0001	0.9035	0.8847	
2FI	0.0032	0.9264	0.9038	
Quadratic	< 0.0001	0.9951	0.9929	Suggested
Cubic	0.0007	0.9972	0.9959	Aliased

Table 5 presents the findings from the analysis of variance (ANOVA) for the quadratic model. The *F-value* of the model stands at 1298.74, which is significantly higher than 0.0001. This value shows that the model is significant. The importance of each element was assessed by analyzing the *F-value* and *p-value*. A *p-value* lower than 0.05 suggests that the model is statistically significant. The higher the *F-value* and the lower the *p-value*, the more significant the corresponding coefficient term is. The terms related to A-concentration and B-temperature were statistically significant, exhibiting *F-values* of 5673.93 and 504.95, respectively. Table 5 demonstrates that the viscosity of XG solution is notably impacted by both concentration and temperature.

Table 5. Output ANOVA from model quadratic

Source	Sum of Squares	df	Mean Square	F-value	p-value	
Model	0.0001	5	0.0000	1298.74	< 0.0001	significant
A-C	0.0000	1	0.0000	5673.93	< 0.0001	
B-T	3.950E-06	1	3.950E-06	504.95	< 0.0001	
AB	1.214E-06	1	1.214E-06	155.15	< 0.0001	
A^2	3.153E-06	1	3.153E-06	402.99	< 0.0001	
B^2	3.872E-08	1	3.872E-08	4.95	0.0346	
Residual	2.112E-07	27	7.823E-09			
Cor Total	0.0001	32				

The adjusted R^2 value of 0.9951 aligns closely with the predicted R^2 value of 0.9929 (Table 6). The difference is under 0.2 in this situation. Given that the value exceeds 4, an adequate precision of 117.8661 is desirable. The outcomes of this model demonstrate a strong degree of consistency, guaranteeing that they are accurate and reliable.

Table 6. Coefficient of regression

Std. Dev.	Mean	CV %	R^2	Adjusted R^2	Predicted R^2	Adeq Precision
0.0001	0.0020	4.37	0.9959	0.9951	0.9929	117.8661

The correlation between the independent variables (*C* and *T*) and the dependent variable (viscosity) under controlled laboratory conditions has been assessed using Eq. (4):

$$Vis = 0.002025 + 2.81162*10^{-6}C - 0.0000617T - 7.59430*10^{-8}CT + 3.79949*10^{-9}C^2 + 7.26682*10^{-7}T^2 \quad (4)$$

Fig. 3 indicates a perturbation chart that shows how two variables influence the viscosity response. The plot is created by perturbing one factor at a time while keeping the other variables unchanged and noting the resulting effects on the response. This enables the visualization of the response surface's curvature and the detection of any interactions among the variables. The slope of each line represents how responsive the result is to that particular variable, whereas the curvature of the line suggests whether there are interactions with other factors. Fig. 3 shows that factor A has the greatest impact on viscosity, whereas factor B has the smallest impact.

With respect to temperature and concentration variables, Fig. 4 illustrates the ratio of normal probability to studentized residuals for the XG solution. The closeness of data to a line can be utilized to assess the appropriateness of the design model. The data points meet the criteria established by the red line. The outcomes fall within the designated range, suggesting that the model created functioned adequately.

Fig. 5 illustrates a comparison between the results gained from experimental analysis and the outcomes predicted by the correlation recommended by RSM. Fig. 5 shows that the real and forecasted outcomes are quite comparable, with only a few very minor discrepancies. The experimental and predicted values are grouped along the normality line in Fig. 5, which verifies the reliability of the analytical system.

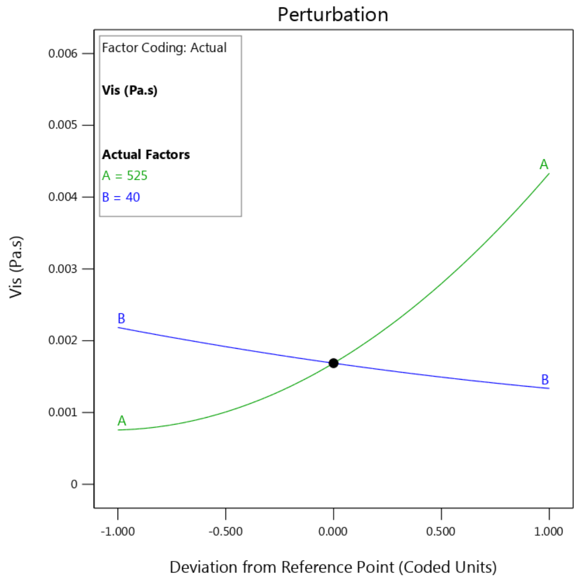

Fig. 3. Perturbation plot of the influence of input factors on the viscosity of the XG solution

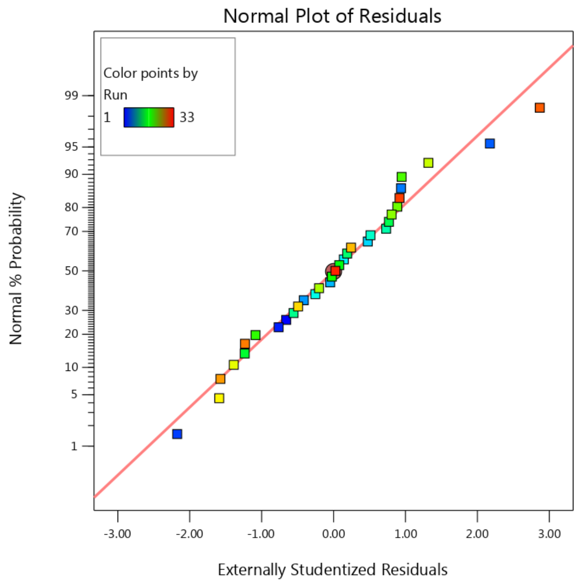

Fig. 4. Normal distribution curve versus residual values

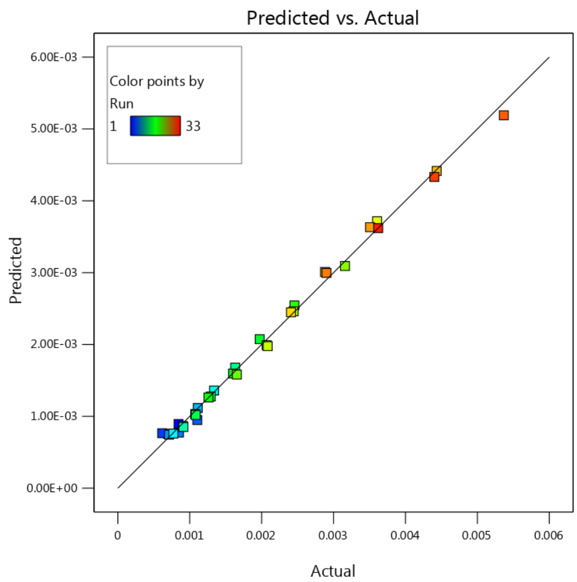

Fig. 5. Comparison of predicted and actual values

The distribution of studentised residuals can be found in Fig. 6a, where the majority of the residuals are clustered near the '0' reference line. This indicates that the established correlations are accurate and that the models effectively represented the behavior of the data. Additionally, in Fig. 6b, a fairly random distribution of residuals throughout the run order is evident, indicating that the model sufficiently addresses the temporal dimension of the data.

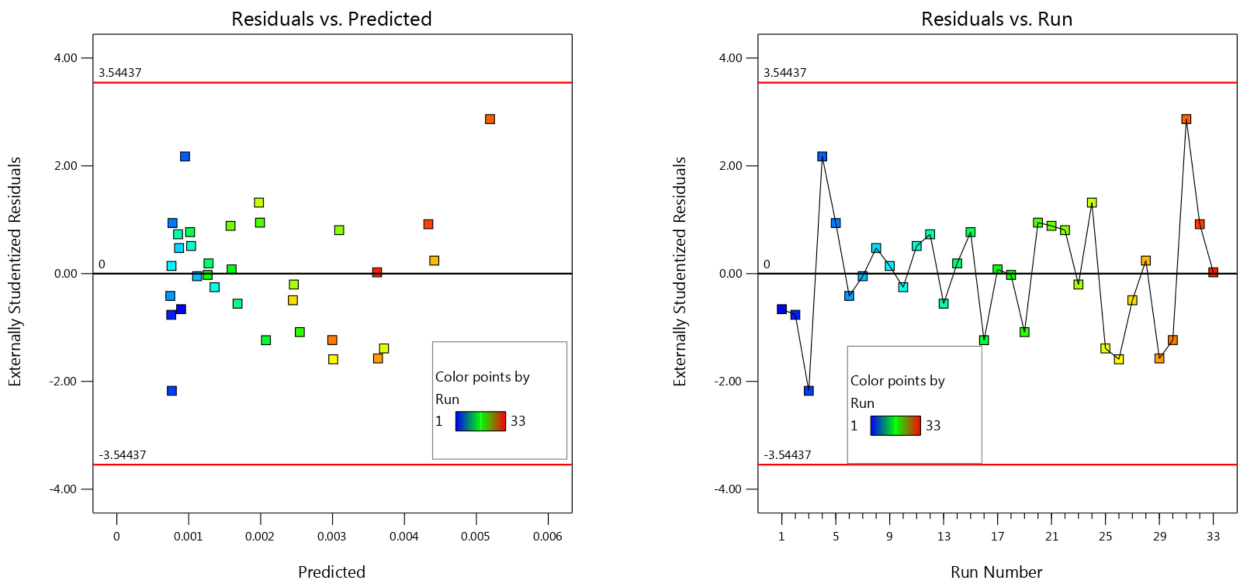

(a) **(b)**

Fig. 6. Plot of externally studentised residuals in relation to (a) predicted value, (b) run order

The 2D contour and 3D surface plots presented in Figs. 7 and 8 demonstrate the influence of various input parameters on the viscosity of the aqueous XG solution. Fig. 7 presents a two-dimensional contour plot that demonstrates how concentration and temperature affect viscosity, aiding in our comprehension of their relationship. Alternatively, Fig. 8 enhances comprehension by displaying a three-dimensional surface plot, which allows for a more in-depth visualization of the intricate relationship among concentration, temperature, and viscosity.

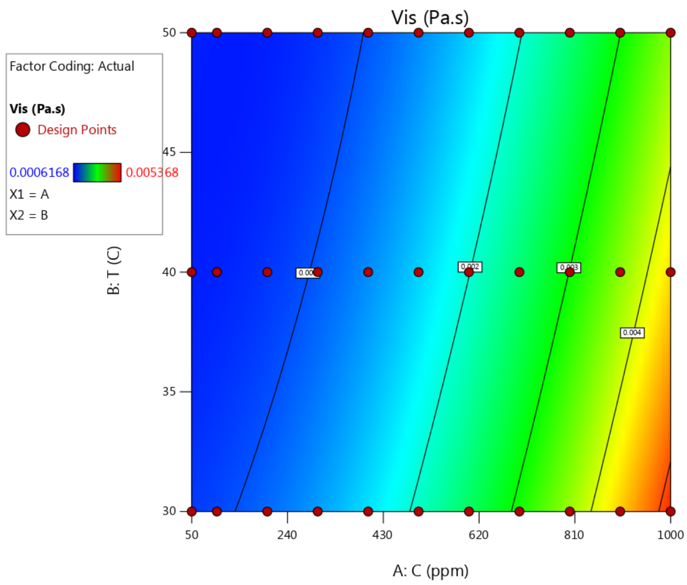

Fig. 7. 2D contour plot of the impact of concentration and temperature on the viscosity of the aqueous XG solution

The contour lines on the plot link locations that share the same viscosity value, helping us to pinpoint areas of higher or lower viscosity and to discover any trends or patterns. The provided plots signify that the viscosity of the aqueous XG solution increases sharply with rising concentration levels. Nonetheless, the influence of increasing concentration on viscosity is more remarkable at lower temperatures. Furthermore, a rise in temperature causes a reduction in viscosity. As the temperature rises, the distance between polymer particles and the molecules of the base fluid expands, resulting in weakened intermolecular forces. This allows the layers of the polymer solution to slip more freely over one another, leading to a reduction in viscosity.

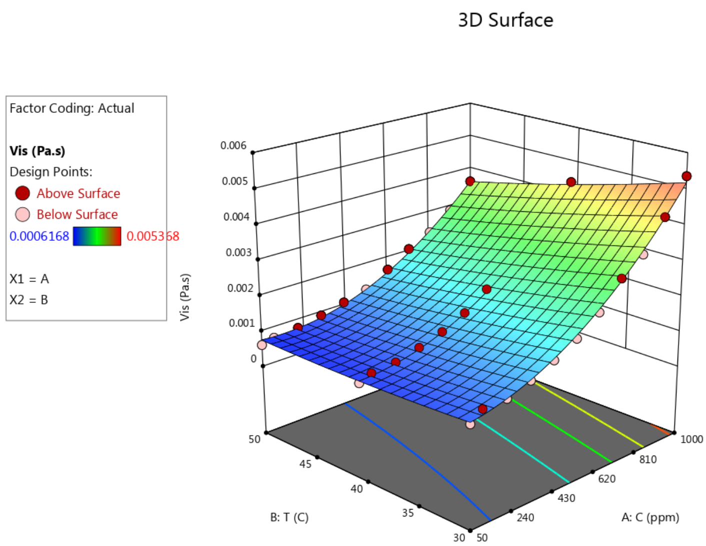

Fig. 8. 3D contour plot of the impact of concentration and temperature on the viscosity of the aqueous XG solution

4.2. Correlations comparison

The experimental results were evaluated against the forecasts made by existing models, both theoretical and experimental, that had been suggested by researchers earlier; this is illustrated in Table 7. The effectiveness of these models is assessed using the Average Absolute Relative Deviation (AARD) by comparing it with experimental data according to Eq. (5), and the results are outlined in Table 7:

$$AARD\% = \frac{100}{N}\sum_{i=1}^{N}\frac{\left[\mu_{exp}^{i} - \mu_{pred}^{i}\right]}{\mu_{exp}^{i}} \tag{5}$$

The AARD of these models in forecasting the viscosity of the studied polymeric solution varied between 53.923 and 58.229%, which indicates an unacceptable error. This is while the proposed equation (RSM) shows an AARD of less than 5.4%. In other words, the aqueous XG solution viscosity prediction error has been improved by approximately 11 times compared to the literature equations.

Table 7. Correlation comparison according to AARD

Correlation	AARD (%)
Einstein [54]	53.924
Brinkman [55]	53.923
Lundgren [56]	53.925
Pak&Cho [57]	53.534
Maiga et al. [58]	53.872
Gherasim et al. [59]	58.229
RSM (present study)	5.39

In order to assess the validity of the suggested correlation, experimental data regarding the viscosity of polymer solutions at varying volume concentrations and temperatures (in this section, only results at a temperature of 50°C are presented) were compared by comparing the margin of deviation (MOD) as computed using Eq. (6),([60-62]):

$$\text{Margin of deviation } (\%) = \frac{\mu_{exp} - \mu_{pred}}{\mu_{exp}} \times 100 \quad (6)$$

Fig. 9 shows the deviation between the values predicted by the RSM equation and those obtained from experimental data at different concentrations. The MOD of this model in forecasting the viscosity of the examined polymeric solution ranged from -21.9 to 8.1%. The maximum MOD is for the lowest concentration, 50ppm. This demonstrates an increased level of accuracy in forecasting the viscosity of the examined polymer solution in comparison to the prior models. Hence, the suggested correlation is capable of predicting the viscosity of aqueous XG solution within a temperature range of 30 to 50°C and concentrations between 50 and 1000ppm.

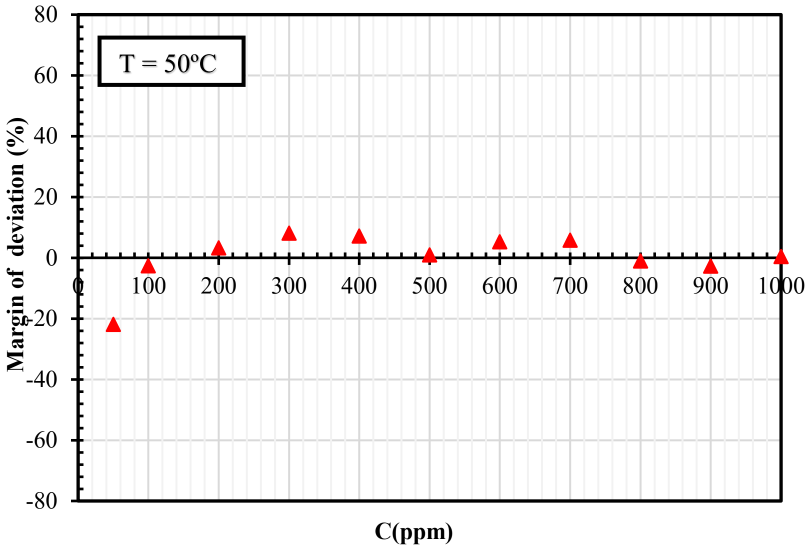

Fig. 9. Margin of deviation for the comparison between experimental values and those obtained from the correlation

In order to examine the feasibility of using the proposed equation of the present research to predict the viscosity of other water-soluble drag reducing polymers, experimental data from the existing literature was compared with predicted results from the RSM model (Table 8). Except for the findings from Raei&Peyghambarzadeh [32] (for XG), the MOD of the enhancement of viscosity of water-soluble drag reducing polymers was < ±19%. Therefore, the RSM model is a strong predictor of the viscosity of water-soluble drag reducing polymers.

Table 8. Comparison of result from Equation (4) and data obtained from literature.

Source	polymer	Temperature (°C)	Concentration (ppm)	Experimental result (Pa.s)	Predicted result (Pa.s)	MOD (%)
Raei&Peyghambarzadeh[32]	XG	50	100	0.000542	0.000731147	-34.9
Raei&Peyghambarzadeh [32]	CMC	50	200	0.00066	0.000746579	-13.1
Raei&Peyghambarzadeh [32]	PAM	50	100	0.00063	0.000731147	-16.1
Raei&Peyghambarzadeh [32]	GG	50	500	0.00105	0.001248813	-18.8
Raei&Peyghambarzadeh [32]	PAA	50	100	0.00083	0.000731147	11.9
Varnaseri et al.[63]	PAM	70	150	0.001266	0.001025572	18.9
Varnaseri&Peyghambarzadeh [53]	PAM	65	100	0.0010419	0.000955759	8.3
Varnaseri&Peyghambarzadeh [53]	XG	65	100	0.0010748	0.000955759	11

5. Conclusion

In this study, we conducted experimental and statistical analysis on the dynamic viscosity of aqueous XG solution by employing RSM. The use of RSM in the research proved to be successful, resulting in an equation that provides accurate forecasts for the dynamic viscosity of the aqueous XG solution. RSM offered various equations for determining viscosity depending on separate factors like C and T. The quadratic model has proven to be more effective than other models by analyzing statistical parameters and plots. The values for R^2, adjusted R^2, predicted R^2, and Std. Dev in the quadratic model were 0.9959, 0.9951, 0.9929, and 0.0001 respectively. The difference between adjusted R^2 and predicted R^2 is under 0.003, demonstrating the high accuracy of the suggested model. The residual plot, the normal probability plot, and the predicted versus actual plot all indicated that the quadratic model is highly accurate and proficient in forecasting the viscosity of an aqueous XG solution. The provided plots signify that the viscosity of the aqueous XG solution increases sharply with rising concentration levels. Nonetheless, the influence of increasing concentration on viscosity is more remarkable at lower temperatures. Furthermore, a rise in temperature causes a reduction in viscosity. As the temperature rises, the distance between polymer particles and the molecules of the base fluid expands, resulting in weakened intermolecular forces. This allows the layers of the polymer solution to slip more freely over one another, leading to a reduction in viscosity. Finally, the predictive quality of the proposed model was evaluated using experimental data from the literature. The outcomes displayed that the proposed model can predict the viscosity of water-soluble DRA with acceptable accuracy, with a relative deviation of less than 19%.

Nomenclature

Symbols

C	Concentration
d	Regression coefficient
h	hour
T	Temperature

Abbreviations

AARD	Average absolute relative deviations
CMC	Carboxymethyl cellulose
CV	Coefficient of variation
DG	Diutan gum
DR	Drag reduction
DRAs	Drag reducing agents
DRPs	Drag reducing polymers
DW	Deionised water
GG	Guar gum
Mw	Molecular weight
NA	Not available
ppm	Parts per million
PAM	Polyacrylamide
PEO	Polyethylene oxide
RSM	Response surface metodology
Std.Dev	Standard deviation
XG	Xanthan gum

Greek symbols

ρ	Density
μ	Viscosity

Subscripts

bf	base fluid
exp	experimental
p	polymer
pred	predicted

References

[1] Toms, B.A., 1948. Some observations on the flow of linear polymer solutions through straight tubes at large Reynolds number. In: Proceedings of the First International Congress on Rheology. North Holland, Amsterdam.
[2] Soares, E.J., 2020. Review of mechanical degradation and de-aggregation of drag reducing polymers in turbulent flows. Journal of Non-Newtonian Fluid Mechanics, 276, 104225. https://doi.org/10.1016/j.jnnfm.2019.104225
[3] Saeed, Z., Elbing, B.R., 2023. Polymer drag reduction: A review through the lens of coherent structures in wall-bounded turbulent flows. Physics of Fluids, 35(8). https://doi.org/10.1063/5.0162648
[4] White, C.M., Mungal, M.G., 2008. Mechanics and prediction of turbulent drag reduction with polymer additives. Annual Review of Fluid Mechanics, 40(1), 235–256. https://doi.org/10.1146/annurev.fluid.40.111406.102156
[5] Ptasinski, P., Nieuwstadt, F., Van Den Brule, B., Hulsen, M., 2001. Experiments in turbulent pipe flow with polymer additives at maximum drag reduction. Flow, Turbulence and Combustion, 66(2), 159–182. https://doi.org/10.1023/A:1017985826227
[6] Mohammadtabar, M., Sanders, R., Ghaemi, S., 2020. Viscoelastic properties of flexible and rigid polymers for turbulent drag reduction. Journal of Non-Newtonian Fluid Mechanics, 283, 104347. https://doi.org/10.1016/j.jnnfm.2020.104347
[7] dos Santos, W.R., Caser, E.S., Soares, E.J., Siqueira, R.N., 2020. Drag reduction in turbulent flows by diutan gum: A very stable natural drag reducer. Journal of Non-Newtonian Fluid Mechanics, 276, 104223. https://doi.org/10.1016/j.jnnfm.2019.104223

[8] Escudier, M., Nickson, A., Poole, R., 2009. Turbulent flow of viscoelastic shear-thinning liquids through a rectangular duct: Quantification of turbulence anisotropy. Journal of Non-Newtonian Fluid Mechanics, 160(1), 2–10. https://doi.org/10.1016/j.jnnfm.2009.01.002
[9] Warwaruk, L., Ghaemi, S., 2021. A direct comparison of turbulence in drag-reduced flows of polymers and surfactants. Journal of Fluid Mechanics, 917, A7. https://doi.org/10.1017/jfm.2021.264
[10] Soares, E.J., Sandoval, G.A., Silveira, L., Pereira, A.S., Trevelin, R., Thomaz, F., 2015. Loss of efficiency of polymeric drag reducers induced by high Reynolds number flows in tubes with imposed pressure. Physics of Fluids, 27(12). https://doi.org/10.1063/1.4937594
[11] Pereira, A.S., Andrade, R.M., Soares, E.J., 2013. Drag reduction induced by flexible and rigid molecules in a turbulent flow into a rotating cylindrical double-gap device: Comparison between poly(ethylene oxide), polyacrylamide, and xanthan gum. Journal of Non-Newtonian Fluid Mechanics, 202, 72–87. https://doi.org/10.1016/j.jnnfm.2013.09.008
[12] Den Toonder, J., Draad, A., Kuiken, G., Nieuwstadt, F., 1995. Degradation effects of dilute polymer solutions on turbulent drag reduction in pipe flows. Applied Scientific Research, 55(1), 63–82. https://doi.org/10.1007/BF00854224
[13] Lim, G.H., Choi, H.J., Renou, F., Roy, A.N., 2017. Effects of hydrophobic modification of xanthan gum on its turbulent drag reduction characteristics. Journal of Industrial and Engineering Chemistry, 54, 146–150. https://doi.org/10.1016/j.jiec.2017.05.027
[14] Sandoval, G.A., Soares, E.J., 2016. Effect of combined polymers on the loss of efficiency caused by mechanical degradation in drag reducing flows through straight tubes. Rheologica Acta, 55(7), 559–569. https://doi.org/10.1007/s00397-016-0927-6
[15] Rajappan, A., McKinley, G.H., 2019. Epidermal biopolysaccharides from plant seeds enable biodegradable turbulent drag reduction. Scientific Reports, 9(1), 18263. https://doi.org/10.1038/s41598-019-54521-3
[16] Chen, Y., Niu, P., He, M., Li, C., Nechval, A.M., Valeev, A.R., Yang, P., 2025. Turbulent drag reduction behavior of polymer solutions in different geometries. Energy, 323, 135798. https://doi.org/10.1016/j.energy.2025.135798
[17] Chen, Y., Lin, X., He, M., Yang, P., Li, C., Nechval, A.M., Valeev, A.R., 2025. An experimental investigation on the turbulent drag reduction effect of polyacrylamide solution in the loop pipe. Journal of Pipeline Science and Engineering, 100264. https://doi.org/10.1016/j.jpse.2025.100264
[18] Xu, J., Zhou, N., Zhang, J., Yao, Y., Wang, H., Liu, S., 2025. Study on rheological properties of large particle gangue slurry and its drag reduction effect caused by wall slippage in pipeline transportation. Powder Technology, 452, 120573. https://doi.org/10.1016/j.powtec.2024.120573
[19] Barbosa, K.C.O., Soares, E.J., Khalil, M.C., Karnitz, O., 2025. Polymer drag reduction in dispersed oil–water flow in tubes. International Journal of Multiphase Flow, 183, 105064. https://doi.org/10.1016/j.ijmultiphaseflow.2024.105064
[20] Zhou, Z., Li, M., Ge, Z., Zhang, X., Tang, Y., Cui, J., Gong, S., 2025. Drag reduction characteristics of RJD-suitable surfactant-polymer composite fluids under high shear. International Communications in Heat and Mass Transfer, 160, 108341. https://doi.org/10.1016/j.icheatmasstransfer.2024.108341
[21] Shi, P.-F., Hu, H.-B., Wen, J., Xie, L., 2024. Drag reduction and degradation of binary polymer solutions. Journal of Non-Newtonian Fluid Mechanics, 105279. https://doi.org/10.1016/j.jnnfm.2024.105279
[22] Brandfellner, L., Muratspahić, E., Bismarck, A., Müller, H.W., 2024. Quantitative description of polymer drag reduction: Effect of polyacrylamide molecular weight distributions. Journal of Non-Newtonian Fluid Mechanics, 325, 105185. https://doi.org/10.1016/j.jnnfm.2024.105185
[23] Cheng, Z., Zhang, P., Wang, X., Song, X., Dai, X., Gao, L., Zhang, X., Zhang, G., Lu, Y., 2024. Drag reduction and degradation by sodium alginate in turbulent flow. Scientific Reports, 14(1), 16854. https://doi.org/10.1038/s41598-024-67873-2
[24] Fang, M., Li, X., Kong, H., Li, M., Hu, Z., Liu, X., 2025. Advances of two-dimensional materials on drag reduction: Mechanisms and applications. Nano Materials Science. https://doi.org/10.1016/j.nanoms.2025.06.006
[25] Chin, C.H., Kazi, S.N., Zubir, M.N.M., Siew, B.K., Shaikh, K., 2025. Performance improvement of heat transfer and drag reduction through pristine polymer gum arabic and gum karaya and their hybrid in circular pipe flow. Journal of Thermal Analysis and Calorimetry, 1–16. https://doi.org/10.1007/s10973-025-14336-z
[26] Chang, A., Huang, L., Wei, S., Shao, M., 2024. Analysis of the drag reduction performance and rheological properties of drag-reducing additives. Polymers, 16(9), 1247. https://doi.org/10.3390/polym16091247
[27] Zhang, X., Cheng, Z., Dai, X., Xin, Y., Liu, K., Lin, M., Liang, Y., Xiao, Y., Lu, Y., Zhang, G., Qin, X., Zhang, J., 2025. Eco-friendly sodium alginate for drag reduction in hydraulic fracturing: Experimental and FFT-based dynamic analysis. International Journal of Biological Macromolecules, 147945. https://doi.org/10.1016/j.ijbiomac.2025.147945
[28] Vu, L.T.T., Nguyen, C.T., Duong, M.T., Tran, T.D., Pham, T.T.H., Tran, M.T., Ly, L.T.N., Thai, H., 2024. Chrysophanol-loaded composites with xanthan gum/polycaprolactone for drug release enhancement. ChemistrySelect, 9(34), e202402196. https://doi.org/10.1002/slct.202402196
[29] Bhat, I.M., Wani, S.M., Mir, S.A., Masoodi, F., 2022. Advances in xanthan gum production, modifications and its applications. Biocatalysis and Agricultural Biotechnology, 42, 102328. https://doi.org/10.1016/j.bcab.2022.102328
[30] Holzwarth, G., 1976. Conformation of the extracellular polysaccharide of Xanthomonas campestris. Biochemistry, 15(19), 4333–4339.
[31] Patel, J., Maji, B., Moorthy, N.H.N., Maiti, S., 2020. Xanthan gum derivatives: Review of synthesis, properties and diverse applications. RSC Advances, 10(45), 27103–27136. https://doi.org/10.1039/D0RA04366D
[32] Raei, B., Peyghambarzadeh, S.M., 2021. Experimental investigation of drag reduction in turbulent flow using biological and synthetic macromolecules: A comparative study. Journal of Chemical and Petroleum Engineering, 55(1), 117–137. https://doi.org/10.22059/jchpe.2021.307767.1323

[33] Li, J., Zhang, Y., Zhang, D., Liu, C., Kang, J., Li, N., Pan, S., Zhou, F., 2024. Effect of temperature on the drag reduction characteristics of xanthan gum in the liquid ring vacuum pump. Vacuum, 229, 113523. https://doi.org/10.1016/j.vacuum.2024.113523
[34] Abdulbari, H.A., Ling, F.W., Hassan, Z., Thin, H.J., 2018. Experimental investigations on biopolymer in enhancing the liquid flow in microchannel. Advances in Polymer Technology, 37(8), 3136–3145. https://doi.org/10.1002/adv.22084
[35] Abdulbari, H.A., Amir, R., 2021. Drag reduction performance and stability of an organic polymer, surfactant, and their complexes. Chemical Engineering & Technology, 44(12), 2333–2340. https://doi.org/10.1002/ceat.202100073
[36] Li, E., Zheng, L., Li, Y., Fan, L., Zhao, S., Liu, S., 2022. Investigation of the drag reduction of hydrolyzed polyacrylamide–xanthan gum composite solution in turbulent flow. Asia-Pacific Journal of Chemical Engineering, 17(5), e2791. https://doi.org/10.1002/apj.2791
[37] Karami, H.R., Rahimi, M., Ovaysi, S., 2018. Degradation of drag reducing polymers in aqueous solutions. Korean Journal of Chemical Engineering, 35(1), 34–43. https://doi.org/10.1007/s11814-017-0264-1
[38] Choi, H.J., Kim, C.A., Sohn, J.-I., Jhon, M.S., 2000. An exponential decay function for polymer degradation in turbulent drag reduction. Polymer Degradation and Stability, 69(3), 341–346. https://doi.org/10.1016/S0141-3910(00)00080-X
[39] Habibpour, M., Clark, P.E., 2017. Drag reduction behavior of hydrolyzed polyacrylamide/xanthan gum mixed polymer solutions. Petroleum Science, 14(2), 412–423. https://doi.org/10.1007/s12182-017-0152-7
[40] Mitishita, R.S., Elfring, G.J., Frigaard, I.A., 2023. Statistics and spectral analysis of turbulent duct flows with flexible and rigid polymer solutions. Journal of Non-Newtonian Fluid Mechanics, 311, 104952. https://doi.org/10.1016/j.jnnfm.2022.104952
[41] Novelli, G.L., Ferrari, L.A., Vargas, G.G., Loureiro, B.V., 2019. A synergistic analysis of drag reduction on binary polymer mixtures containing guar gum. International Journal of Biological Macromolecules, 137, 1121–1129. https://doi.org/10.1016/j.ijbiomac.2019.07.042
[42] Habibpour, M., Koteeswaran, S., Clark, P.E., 2017. Drag reduction behavior of hydrolyzed polyacrylamide/polysaccharide mixed polymer solutions: Effect of solution salinity and polymer concentration. Rheologica Acta, 56(7–8), 683–694. https://doi.org/10.1007/s00397-017-1024-1
[43] Akindoyo, E.O., Abdulbari, H., 2016. Investigating the drag reduction performance of rigid polymer–carbon nanotubes complexes. Journal of Applied Fluid Mechanics, 9(3), 1041–1049. https://doi.org/10.18869/acadpub.jafm.68.228.24332
[44] Peyghambarzadeh, S., Hashemabadi, S., Saffarian, H., Shekari, F., 2016. Experimental study of the effect of drag reducing agent on pressure drop and thermal efficiency of an air cooler. Heat and Mass Transfer, 52(1), 63–72. https://doi.org/10.1007/s00231-015-1650-z
[45] Raei, B., Shahraki, F., Peyghambarzadeh, S.M., 2018. Experimental study of the effect of drag reducing agent on heat transfer and pressure drop characteristics. Experimental Heat Transfer, 31(1), 68–84. https://doi.org/10.1080/08916152.2017.1353557
[46] Cheng, Z., Zhang, X., Song, X., Wang, X., Zhang, G., Lu, Y., Li, L., Liu, F., Dai, X., 2023. Investigation of drag reduction by slurry-like drag-reducing agent in microtube flow using response surface methodology (RSM). Scientific Reports, 13(1), 22433. https://doi.org/10.1038/s41598-023-49804-9
[47] Raei, B., 2025. Using response surface methodology (RSM) to evaluate the drag reduction by polyacrylamide: Experimental and statistical investigation. Chemical Process Design, 4(1), 44–59. https://doi.org/10.22111/cpd.2025.51346.1051
[48] Raei, B., 2023. The effect of polymeric drag reducing agent on pressure drop reduction in circular pipes: Experimental and statistical investigation. Journal of the Indian Chemical Society, 100(3), 100905. https://doi.org/10.1016/j.jics.2023.100905
[49] Teng, T.-P., Hung, Y.-H., Teng, T.-C., Mo, H.-E., Hsu, H.-G., 2010. The effect of alumina/water nanofluid particle size on thermal conductivity. Applied Thermal Engineering, 30(14–15), 2213–2218. https://doi.org/10.1016/j.applthermaleng.2010.05.036
[50] Box, G.E.P., Wilson, K.B., 1992. On the experimental attainment of optimum conditions. In: Breakthroughs in Statistics: Methodology and Distribution. Springer, pp. 270–310. https://doi.org/10.1007/978-1-4612-4380-9_23
[51] Shirvan, K.M., Mamourian, M., Mirzakhanlari, S., Öztop, H.F., Abu-Hamdeh, N., 2016. Numerical simulation and sensitivity analysis of effective parameters on heat transfer and homogeneity of Al2O3 nanofluid in a channel using DPM and RSM. Advanced Powder Technology, 27(5), 1980–1991. https://doi.org/10.1016/j.apt.2016.06.030
[52] Gaitonde, V., Manjaiah, M., Maradi, S., Karnik, S., Petkar, P., Davim, J.P., 2017. Multiresponse optimization in wire electric discharge machining (WEDM) of HCHCr steel by integrating response surface methodology (RSM) with differential evolution (DE). In: Computational Methods and Production Engineering. Elsevier, pp. 199–221. https://doi.org/10.1016/B978-0-85709-481-0.00007-0
[53] Varnaseri, M., Peyghambarzadeh, S., 2020. Comprehensive study of the effect of the addition of four drag reducing macromolecules on the pressure drop and heat transfer performance of water in a finned tube heat exchanger. Journal of Macromolecular Science, Part B, 59(11), 747–773. https://doi.org/10.1080/00222348.2020.1801194
[54] Einstein, A., 1906. A new determination of the molecular dimensions. Annalen der Physik, 19, 289–306.
[55] Brinkman, H.C., 1952. The viscosity of concentrated suspensions and solutions. The Journal of Chemical Physics, 20(4), 571. https://doi.org/10.1063/1.1700493
[56] Lundgren, T.S., 1972. Slow flow through stationary random beds and suspensions of spheres. Journal of Fluid Mechanics, 51(2), 273–299. https://doi.org/10.1017/S002211207200120X
[57] Pak, B.C., Cho, Y.I., 1998. Hydrodynamic and heat transfer study of dispersed fluids with submicron metallic oxide particles. Experimental Heat Transfer, 11(2), 151–170. https://doi.org/10.1080/08916159808946559
[58] Maïga, S.E.B., Nguyen, C.T., Galanis, N., Roy, G., 2004. Heat transfer behaviours of nanofluids in a uniformly heated tube. Superlattices and Microstructures, 35(3–6), 543–557. https://doi.org/10.1016/j.spmi.2003.09.012

[59] Gherasim, I., Roy, G., Nguyen, C.T., Vo-Ngoc, D., 2009. Experimental investigation of nanofluids in confined laminar radial flows. International Journal of Thermal Sciences, 48(8), 1486–1493. https://doi.org/10.1016/j.ijthermalsci.2009.01.008

[60] Karimipour, A., Ghasemi, S., Darvanjooghi, M.H.K., Abdollahi, A., 2018. A new correlation for estimating the thermal conductivity and dynamic viscosity of CuO/liquid paraffin nanofluid using neural network method. International Communications in Heat and Mass Transfer, 92, 90–99. https://doi.org/10.1016/j.icheatmasstransfer.2018.02.002

[61] Khodadadi, H., Toghraie, D., Karimipour, A., 2019. Effects of nanoparticles to present a statistical model for the viscosity of MgO-water nanofluid. Powder Technology, 342, 166–180. https://doi.org/10.1016/j.powtec.2018.09.076

[62] Ezekwem, C., Dare, A., 2022. Experimental investigation on viscosity of AlN and SiC nanofluids. Chemical Engineering Communications, 209(2), 229–245. https://doi.org/10.1080/00986445.2020.1855151

[63] Varnaseri, M., Peyghambarzadeh, S.M., Amiri, M., 2018. Experimental study on optimum concentration of polyacrylamide for drag reduction and heat transfer performance in a compact heat exchanger. Heat and Mass Transfer, 55(4), 1119–1132. https://doi.org/10.1007/s00231-018-02533-6